Research Square

Preprints are preliminary reports that have not undergone peer review.
They should not be considered conclusive, used to inform clinical practice,
or referenced by the media as validated information.

Study on Corrosion Imaging of Aircraft Riveted Structures Based on Pulsed Eddy Current

Qiufeng Li
Nanchang Hangkong University
Rengchuan Qin
Nanchang Hangkong University
Zhibo Wang
Nanchang Hangkong University
Ruiqi. Zhou
Nanchang Hangkong University
Jie Chen
Jiangxi General Institute of Testing and Certification
Xin Li
lixin1924@nuaa.edu.cn

Jiangxi General Institute of Testing and Certification

Research Article

Keywords: Pulsed eddy current, Aircraft riveted structure, Defect detection, Tunnel magnetoresistance sensor array

Posted Date: August 12th, 2026

DOI: https://doi.org/10.21203/rs.3.rs-10179840/v1

License: This work is licensed under a Creative Commons Attribution 4.0 International License.
Read Full License

Additional Declarations: Competing interest reported. Competing Interest Declaration This work was supported in part by the National Key R&D Program (No. 2024YFB3214300), the National Natural Science Foundation of China (No. 12364056), the Natural Science Foundation of Jiangxi Province (Nos. 20253BAC280090 and 20252BAC240318), and the Science and Technology Project of Jiangxi Administration for Market Regulation (No. GSJK202406). The authors have no other relevant financial or non-financial interests to disclose. All authors certify that they have no affiliations with or involvement in any organization or entity with any other financial interest or non-financial interest in the subject matter

or materials discussed in this manuscript. Specifically, the authors declare that they have no other financial interests (including but not limited to research grants, employment, consultancies, stock ownership, honoraria, or patents) that could be perceived as influencing the submitted work, apart from the research grants explicitly listed above. Furthermore, the authors have no non-financial interests (including but not limited to professional relationships, personal beliefs, positions on editorial/advisory boards, or expert testimony) that could impart bias on the work. The authors have no conflicts of interest to declare that are relevant to the content of this article, and they have no financial or proprietary interests in any material discussed in this article, other than the acknowledged funding sources. The authors confirm that any undeclared financial or non-financial interest that could embarrass them were it to become publicly known after the work was published does not exist. This disclosure statement covers the period of conducting the research and preparing the work for submission, as well as any interests within the last three years that could reasonably be perceived as influencing the submitted work.. Xin Li Nanchang Hangkong University Institute of Special Equipment Inspection and Research, Jiangxi General Institute of Testing and Certification

Study on Corrosion Imaging of Aircraft Riveted Structures Based on Pulsed Eddy Current

Qiufeng Li [1], Rengchuan Qin [1], Zhibo Wang [1], Ruiqi Zhou[1], Jie Chen[2]， Xin Li*[2]

[†]*Key Laboratory of Nondestructive Testing Technology of the Ministry of Education, Nanchang Hangkong University, Qianhu Campus, Nanchang, China.*

**E-mail: lixin1924@nuaa.edu.cn*

[1]*Key Laboratory of Nondestructive Testing Technology of the Ministry of Education*

[2]*Institute of special equipment inspection and research, Jiangxi General Institute of Testing and Certification*

Abstract: Precise quantification of minute defects in pulsed eddy current (PEC) testing is fundamentally limited by the broadening of defect boundary response signals caused by eddy current field diffusion — a key factor that undermines detection accuracy. To improve quantification precision for such small defects, this paper introduces an adaptive power-law sharpening signal processing approach. This method incorporates an algorithm that dynamically tunes the power-law exponent γ according to normalized peak height, thereby compressing the edges of the response envelope and reducing the impact of boundary effects. Subsequently, piecewise cubic Hermite interpolating polynomial (PCHIP) interpolation is applied to generate a high-density data field. This data field is then combined with K-means clustering for automatic segmentation of the defect region, enabling precise extraction of both the area and two-dimensional coordinates. Experiments were conducted using a pulsed eddy current array sensor to detect multi-layer riveted blocks containing corrosion defects. Experimental results verify that the proposed method effectively suppresses the adverse effects of eddy current diffusion on boundary resolution. For circular corrosion defects with diameters from 5 mm to 12 mm at identical burial depth, the method achieves a relative area error below 16.3% and a localization error within 1.5 mm, significantly outperforming conventional threshold-based approaches. This work provides a systematic signal processing framework that addresses the fundamental limitation of boundary broadening in pulsed eddy current testing, paving the way for high-precision quantification of minute defects.

Keywords: Pulsed eddy current; Aircraft riveted structure; Defect detection; Tunnel magnetoresistance sensor array.

1 Introduction

Aircraft multi-layer riveted structures are prone to hidden corrosion damage at interlayer contact surfaces during long-term service due to environmental corrosion and alternating loads. Such defects can significantly weaken structural connection integrity, induce stress concentration, and even lead to catastrophic delamination failures, posing serious threats to flight safety[1-3]. Consequently, developing high-precision, quantitative non-destructive testing (NDT) techniques suitable for multi-layer structures holds significant engineering importance[4-5].

Pulsed Eddy Current (PEC) technology has emerged as an effective method for detecting corrosion defects in metallic materials due to its deep penetration capability[6-7], high sensitivity, and rich time-domain signal characteristics[8-9]. Unlike far-field eddy current testing[10-12], which often requires specific probe configurations for deep detection, infrared thermography[13-14], susceptible to surface emissivity and environmental interference, or Lamb wave testing[15], typically requiring couplants or specific excitation conditions, PEC technology exhibits insensitivity to surface conditions and eliminates the need for couplants. This makes it particularly suitable for inspecting riveted structures with surface coatings such as paint or sealant[16-17]. Regarding PEC probes[18], Xu et al.[19] proposed a multi-coil sequential excitation strategy, significantly reducing probe size and enhancing its applicability for defect detection in confined spaces within aircraft structures. Yao et al.[20] focused on the signal processing level, introducing a parameter inversion algorithm for PEC signals to precisely quantify thickness loss in ferromagnetic materials caused by corrosion. Wang et al.[21] further employed a dual-sensor differential PEC technique, aiming to achieve high-contrast imaging and quantitative evaluation of subsurface corrosion defects in ferromagnetic metals. To improve inspection efficiency and defect identification accuracy, machine learning shows promise in the non-destructive testing field [22-24]. Vu et al.[25] explored a data-driven approach, designing a lightweight Convolutional Neural Network (CNN) to process magnetic testing data for efficient detection of hidden corrosion in aircraft structures.

In the domain of defect quantitative assessment, researchers have proposed various innovative methods. Addressing the critical challenge of quantifying fatigue natural cracks in aero-aluminum alloys, Sun et al.[26] developed a Pulsed Eddy Current (PEC)-based approach employing a Genetic Algorithm-optimized Back Propagation Neural Network (GA-BPNN). Their method achieved a high characterization accuracy of 2.19% for natural crack depth.For multi-layered structures, Xiao Chen et

al.[27] utilized Pulsed PEC technology to propose a defect classification method based on Fisher Linear Discriminant Analysis (FLDA), which effectively distinguished between surface and subsurface defects. Saleh Hosseini and Aouni A. Lakis[28] employed time-frequency analysis and Principal Component Analysis (PCA) to enhance measurement reliability. They further applied K-means clustering and the Expectation-Maximization (EM) algorithm to classify data and automatically determine the distribution of defects within each layer.Although PEC technology shows promise for inspecting multi-layered structures and research on quantification methods continues to advance, the number of array channels is typically limited due to constraints on probe dimensions and sensor arrangement. This limitation results in relatively low imaging resolution, making it difficult to accurately reconstruct the actual shape of corrosion defects[29-31]. Concurrently, the diffusion effect of eddy current fields near defect boundaries causes the detection signal response area to extend significantly beyond the physical dimensions of the defect, leading to boundary distortion. This phenomenon severely restricts the precise quantitative identification of defect size.

To address these issues and achieve visual detection, quantitative area measurement, and positional localization of interlayer corrosion defects in aircraft multi-layer riveted structures, this paper proposes a corrosion defect quantification method based on TMR (Tunnel MagnetoResistance) array PEC detection. Specifically targeting the issue of defect signal boundary diffusion, an innovative adaptive power-law sharpening algorithm is introduced. This algorithm dynamically adjusts the power-law exponent γ based on normalized peak height, effectively compressing the edges of the response envelope and enhancing boundary localization accuracy. Secondly, to address low-resolution array data, piecewise cubic Hermite interpolating polynomial (PCHIP) interpolation is employed to reconstruct a high-density data field, improving imaging resolution for accurate defect shape restoration. Subsequently, the K-means clustering algorithm is applied for unsupervised segmentation of the reconstructed data, enabling automatic identification and precise extraction of the defect region. Finally, based on the segmentation results, the defect area and the position of its centroid within the scanning coordinate system are quantitatively calculated. This method effectively circumvents the reliance on large amounts of annotated data, providing a novel approach for the high-precision quantitative assessment of hidden corrosion.

Following the introduction, the thesis structure is outlined as follows：

Chapter 2: Methodology details the experimental design, which involves acquiring a reference

signal from a defect-free specimen, subtracting the defect detection signal to obtain the differential signal, and subsequently processing this signal through adaptive power-law sharpening, PCHIP interpolation, and k-means clustering to extract defect area and coordinates. This chapter also elaborates on the adaptive power-law sharpening method, the PCHIP interpolation method, and the k-means clustering method.

Chapter 3: Experimental Setup describes the pulsed eddy current inspection system, the multi-layer riveted structure corrosion defect specimen, and the TMR array probe configuration design and scanning procedure.

Chapter 4: Experimental Results and Discussion presents and analyzes the results of feature extraction and defect imaging, assesses the defect shape restoration capability, and examines the impact of the sharpening process on defect quantification accuracy.

Finally, Chapter 5: Conclusion and Future Work summarizes the key findings and suggests directions for future research.

2 Methodology

2.1 Experimental Design

First, acquire the reference signal from a defect-free specimen. Subtract the defect detection signal from this reference to yield the differential signal. Subsequently, process the signal through adaptive power-law sharpening, PCHIP interpolation, and k-means clustering segmentation to extract the defect area and coordinates. The overall flow is shown in Figure 1.

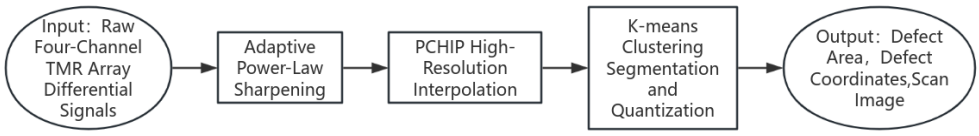


Fig. 1. Technical Framework Flowchart

2.2 Adaptive Power-Law Sharpening Signal Processing Method

Due to the diffusion effect of the electromagnetic field within multi-layer conductive structures, the full width at half maximum (FWHM) of the defect signal is significantly larger than the actual geometric size of the defect. This leads to a reduction in the spatial resolution of the detection signal. To eliminate the edge blurring effect caused by field diffusion, this paper employs an adaptive sharpening algorithm to perform nonlinear compression on the signal envelope.

Firstly, the defect center position is determined through peak detection, and the boundary positions are identified through valley detection. Then, the adaptive sharpening coefficient $\gamma_{adaptive}$ is established, with its formula given as follows:

$$\gamma_{adaptive}=\gamma_{min}+\left(\frac{V_{peak}-V_{min}}{V_{max}-V_{min}}\right)\times(\gamma_{max}-\gamma_{min})+\Delta_{noise},\ \Delta_{noise}\in[-0.2,0.2] \quad (1)$$

Where: V_{peak} represents the amplitude of the currently processed peak; V_{min} and V_{max} represent the minimum and maximum values of all peaks in the signal sequence; γ_{min}=1.5 (lower limit for weak sharpening), γ_{max}=3.0 (upper limit for strong sharpening); Δ_{noise} is the random noise term.

The sharpening formula for the signal rising edge is:

$$norm_rise=\frac{y_{rise}-V_{left}}{V_{peak}-V_{left}} \quad (2)$$

$$y_{sharp_rise}=(norm_rise)^{\gamma_{adaptive}}\times(V_{peak}-V_{left})+V_{left} \quad (3)$$

Where: $norm_rise$ denotes the normalized rising-edge signal; y_{rise} represents the actual signal value; y_{sharp_rise} indicates the sharpened rising-edge signal; V_{left} signifies the valley value on the left side of the peak.

The sharpening formula for the signal falling edge is:

$$norm_fall=\frac{y_{fall}-V_{right}}{V_{peak}-V_{right}} \quad (4)$$

$$y_{sharp_fall}=(norm_fall)^{\gamma_{adaptive}}\times(V_{peak}-V_{right})+V_{right} \quad (5)$$

Where: $norm_fall$ represents the normalized falling-edge signal; y_{fall} denotes the actual signal value; y_{sharp_fall} indicates the sharpened falling-edge signal; V_{right} signifies the valley value on the right side of the peak.

2.3 Signal PCHIP Interpolation Method

The original sensor only provides measurement data at four discrete height positions, resulting in significantly insufficient vertical resolution that fails to meet the requirements for fine defect imaging.

To address this, this paper employs the Piecewise Cubic Hermite Interpolating Polynomial (PCHIP) algorithm to perform high-density interpolation on vertically oriented signals at each scanning position. The PCHIP interpolation formula is:

$$p_i(t)=a_i+b_i(t-x_i)+c_i(t-x_i)^2+d_i(t-x_i)^3,\ \ t\in[xi,xi+1]t\in[x_i,x_{i+1}] \quad (6)$$

Where: coefficients a_i, b_i, c_i, d_i denote the constant, linear, quadratic, and cubic term coefficients respectively; x_i represents the position of the i-th original sensor; t indicates the interpolation point position.

2.4 K-Means Clustering Method

K-means clustering is an unsupervised learning algorithm, and its implementation process is illustrated in Figure 2. This algorithm identifies defects by measuring the similarity between samples. During the clustering process, the cluster centers are iteratively updated until the objective function converges within a specified threshold.

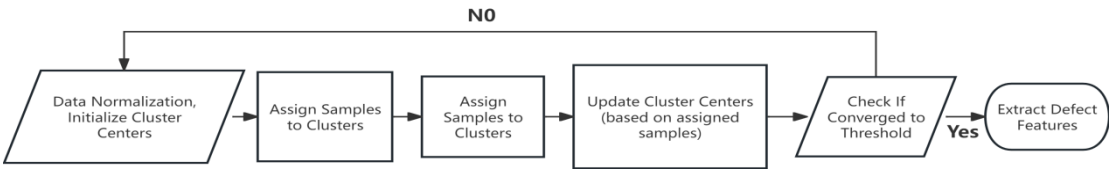


Fig. 2. K-means Clustering Process Flowchart

In this study, the analysis targets are not image pixels but inspection scan points. At each scan step point, an array of four TMR sensors acquires pulsed eddy current signals. The differential signal between the inspection signal and a reference signal is calculated. The peak value of this differential signal and its corresponding peak time point are extracted as core features. These feature signals are organized into a feature matrix, which represents the similarity in signal response across different scan points. This similarity serves as the basis for K-means clustering to delineate defect regions.

3 Experimental Setup

3.1 Pulsed Eddy Current Inspection System

The pulsed eddy current inspection system developed in this study is an integrated experimental platform incorporating excitation signal generation, high-sensitivity sensing, high-speed data acquisition, automated scanning control, and real-time data processing with imaging functions. Figure 3 displays the physical system, and Figure 4 shows the system framework. The system operates via four core modules: the excitation/reception module, detection module, software control and data

processing platform, and automated scanning device.

The excitation/reception module uses a GDF470 function generator to produce square-wave pulse signals (50% duty cycle, 50 Hz repetition frequency) as the excitation source. For driving the detection probe, signals are amplified using the OPA544 power amplifier. Probe response signals undergo low-noise, high-CMRR conditioning via an AD8422 instrumentation amplifier, while an INA199A current-sensing amplifier monitors excitation coil current in real time to ensure stability. Conditioned analog voltage signals are digitized by a USB3133A high-speed data acquisition card at a 100 kHz sampling frequency to precisely capture transient eddy current responses.The detection module employs a customized pulsed eddy current probe applied to aircraft multi-layer metal riveted structures. It excites eddy current fields within the component and captures perturbation signals caused by defects (e.g., corrosion, cracks, or riveting anomalies).The software control and data processing platform, developed in LabVIEW, controls the automated scanning mechanism, acquires and displays real-time eddy current waveforms from the DAQ card, performs online signal processing, and enables immediate defect imaging with data storage.The automated scanning device, comprising a 40-ball-screw linear module and FMDD5040 stepper motor driver, Enables high-precision 2D scanning and positioning across specimen surfaces under LabVIEW control. This integrated system provides reliable hardware support and software environment for defect feature extraction and quantitative evaluation in aircraft multi-layer riveted structures.

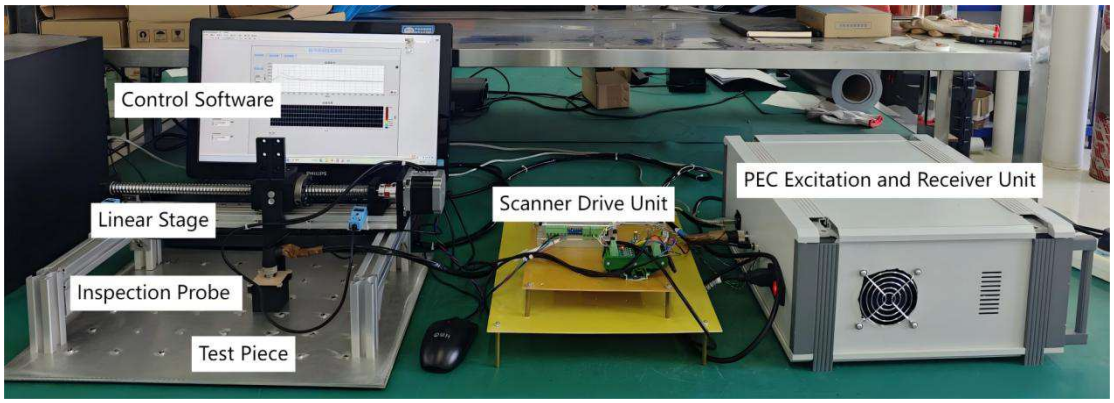


Fig. 3. Physical Setup of Detection System

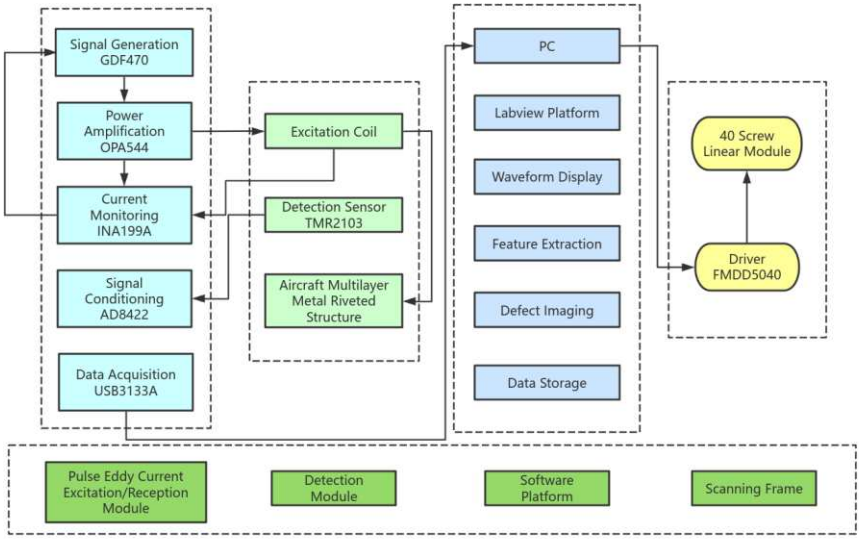
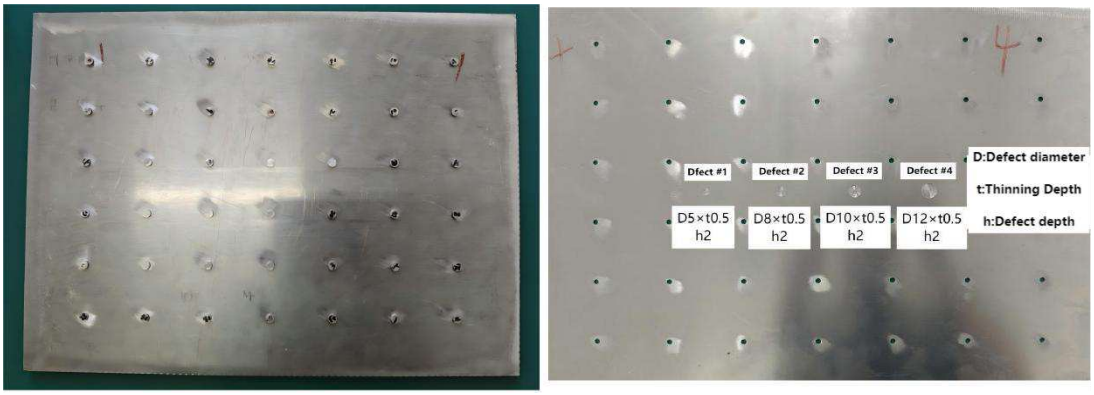


Fig. 4. Block Diagram of Detection System

3.2 Multi-Layer Riveted Structure Corrosion Defect Specimen

The experimental specimen used in this study is a riveted aluminum alloy specimen simulating aircraft multi-layer lap-joint structures, with its specific configuration shown in Figure 5. The specimen consists of five stacked and riveted 6061 aluminum alloy plates, each with unified geometric dimensions of length 480 mm × width 300 mm × thickness 1.0 mm. To evaluate the pulsed eddy current inspection system's detection capability for internal corrosion defects, artificially manufactured defects simulating corrosion damage were prepared.

Defects are located inside the third-layer aluminum plate, with specific parameters listed in Table 1. The upper surface of the defects is at a depth of 2.0 mm from the specimen's inspection surface. The prefabricated defects are circular through-hole thinning defects designed to simulate typical uniform corrosion thinning. Defects are designed with four different diameter specifications: 5 mm, 8 mm, 10 mm, and 12 mm. All defects have a remaining thickness (i.e., thinning depth) of 0.5 mm, representing 50% thinning relative to the original plate thickness (1.0 mm). This specimen design can be used to study the system's detection sensitivity for defects of different sizes and defect resolution at a specific depth (2 mm).



(a) Surface of the riveted component **(b) Circular corrosion defect**

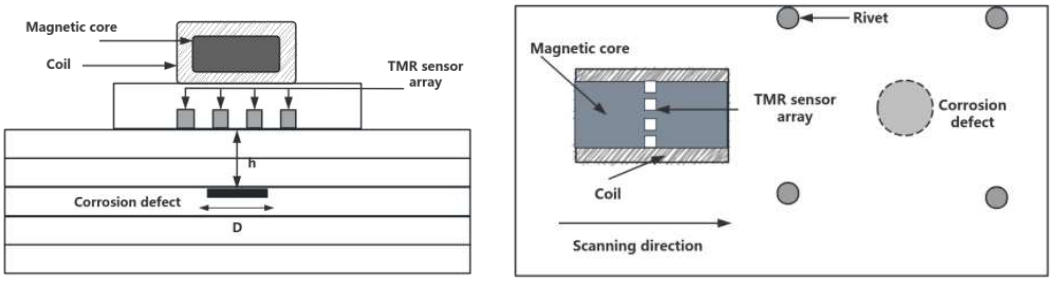
Fig. 5. Test Block Samples with Artificial Defects

Table 1 Corrosion Defect Parameters

Parameters	Defect#1	Defec#2	Defec#3	Defec#4
Diameter×Thinning Depth×Defect depth / mm	5×0.5×2	8×0.5×2	10×0.5×2	12×0.5×2

3.3 TMR Array Probe Configuration Design and Corrosion Defect Scanning

The probe in this paper is shown in Figure 6, with specific parameters listed in Table 2. The probe core employs four TMR2103 tunnel magnetoresistance sensors arranged in a linear array, integrated on a rectangular ferrite magnetic core. High permeability was a key factor in selecting ferrite material, along with its high saturation magnetic flux density, excellent thermal stability, wear resistance, and good customizability. To minimize defect miss rates while accommodating PCB design constraints, the sensor chips adopt a densely packed arrangement with a pairwise center-to-center spacing set at the minimum safe distance of 0.5 mm, avoiding signal interference and parasitic capacitance effects.The excitation coil design uses 0.5 mm diameter enameled wire tightly wound in three layers totaling 160 turns around the magnetic core. This turn count resulted from rigorous trade-offs: although increasing turns enhances magnetic field strength and penetration depth, it slows square-wave response, distorts waveforms, enlarges probe size, introduces interference, and reduces resolution; conversely, reducing turns leads to insufficient excitation magnetic energy for effective detection. The final solution prioritizes coil compactness while ensuring adequate magnetic penetration, effectively balancing magnetic field strength, response speed, probe size, and anti-interference performance.



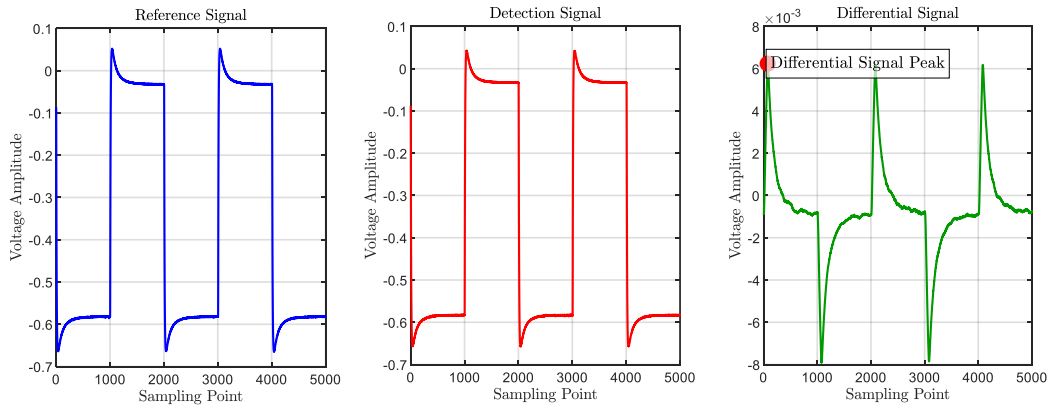
(a) Top view **(b) Side view**

Fig. 6. Schematic Structure of TMR Array Probe

Table 2 Probe Dimension Parameters

Sensor Model	Core Material	Coil Turns / turns	Excitation Coil Enameled Wire Diameter / mm	Center-to-Center Spacing of Sensors / mm	Edge-to-Edge Clearance of Sensors / mm	Probe Overall Dimensions / (L×W×H)mm
TMR2103	Ferrite	160	0.5	3.5	0.5	39mm×38mm×25mm

Reference signals are initially obtained from a defect-free reference area prior to defect detection. After setting the automated scanning frame to move at constant speed, linear scanning is initiated to collect detection signals point-by-point at a step interval of 0.15 mm. To suppress system noise and non-defect interference, differential processing (detection signal - reference signal) is performed on the detection signals at each position, generating high-SNR differential signals as shown in Figure 7. Subsequently, the amplitude peak of the first complete cycle in the differential signal at each scanning point is extracted as the feature value. Upon completing full-area scanning, a peak matrix with dimensions of 4×n (where n is the step count) is ultimately constructed. This matrix stores the feature peak of each point column-wise, providing core input data for subsequent defect imaging and quantitative analysis.



(a) Reference Signal **(b) Detection Signal** **(c) Differential Signal**

Fig. 7. Differential Peak Signal Extraction Process

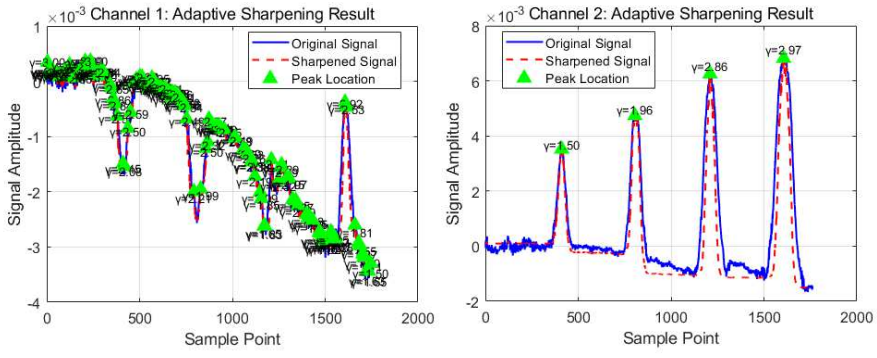
4 Experimental Results and discussion

4.1 Feature Extraction and Defect Imaging

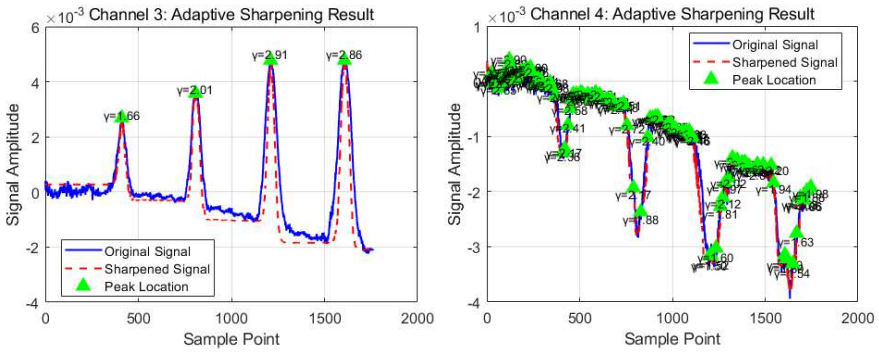
In defect-free regions, the differential signal's baseline amplitude nears zero during detection. As the probe scans to the edge of a defect, the signal amplitude begins to increase nonlinearly, reaches a global maximum at the center of the defect, and then exhibits a monotonically decreasing trend. Overall, this forms a quasi-Gaussian distribution waveform. The sharpened signal is shown in Figure 8.

Channels 1 to 4 represent the signals from four TMR sensors. It is clearly observable that Channels 2 and 3 display four unipolar peaks that first increase and then decrease, corresponding to the four defects respectively. Based on the peak amplitudes of the defect signals, the boundary contours of the circular corrosion defects, approximating their true shapes, were reconstructed by reducing the signal width.

In the Channel 1 signal, three negative unipolar peaks (with amplitudes showing a trend of first decreasing then increasing) and one positive unipolar peak (with amplitude first increasing then decreasing) are visible. The appearance of the negative peaks is attributed to the smaller size of the first three defects, which resulted in the sensitive region of Channel 1's TMR sensor failing to effectively cover the interior region of these defects during scanning. Similarly, since the sensitive region of Channel 4's TMR sensor did not effectively cover the interior region of any of the four defects during scanning, four negative unipolar peaks appeared.



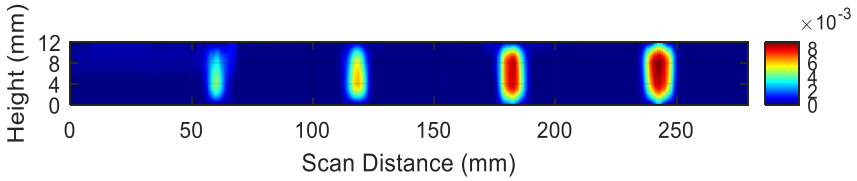
(a) Channel 1 **(b) Channel 2**



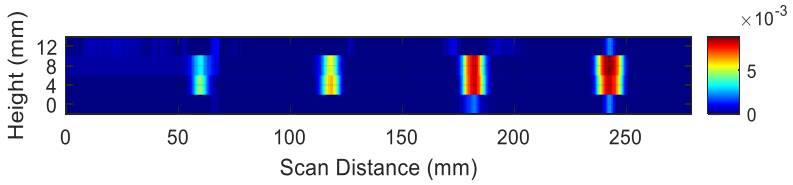
(c) Channel 3 **(d) Channel 4**

Fig. 8. Signal Sharpening Processing Comparison

After PCHIP interpolation processing, data from the four sensors are expanded to 96 points. Figure 9 shows a comparison between non-interpolated imaging and pseudo-color imaging after interpolation completion. It can be clearly observed that the latter exhibits superior edge contours capable of reflecting the specific shape of defects.



(a) Non-interpolated Imaging



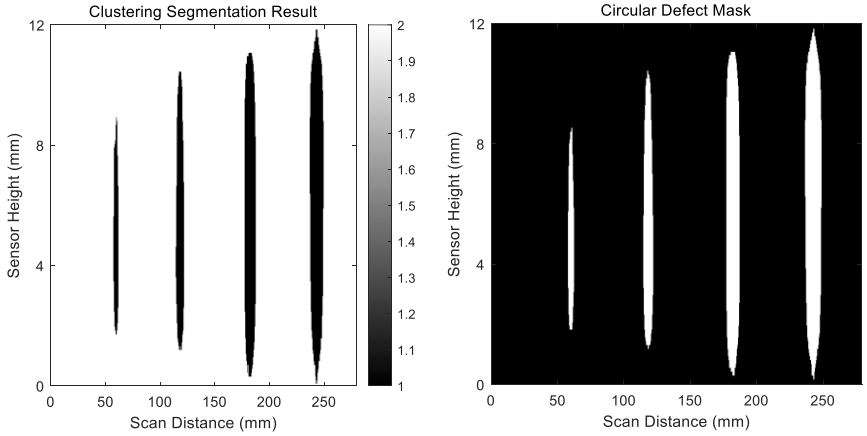
(b) Interpolated Imaging

Fig. 9. Post-Interpolation

In the defect identification stage, the scan distance (x-axis) and sensor height (y-axis) are first normalized to the [0,1] range, transforming the image into actual spatial coordinates.

An improved k-means clustering algorithm is then employed to segment the inspection area into defect and background classes. This algorithm combines data values with spatial coordinate features using squared Euclidean distance, with a maximum of 1000 iterations and 5 repeated runs to ensure stability, as illustrated in Figure 10. Two key parameters are extracted for each defect:Defect Area: Calculated through connected region analysis and conversion using physical resolution to determine actual area.Scan Direction Coordinate: Determined from the centroid position along the x-axis to establish the scan distance.

The final output provides both the area value and precise position coordinate in the scan direction for each detected circular defect, as shown in Figure 11.



(a) Clustering Segmentation **(b) Circular Defect Mask**

Fig. 10. Defect Segmentation Results via k-means Clustering

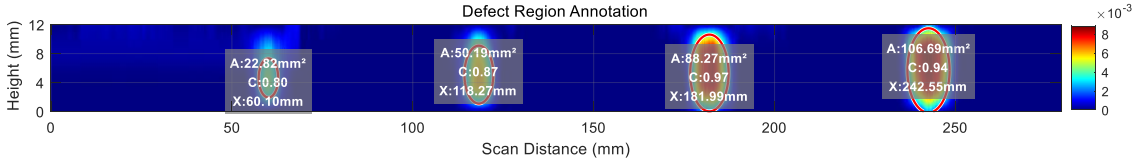


Fig. 11. Defect Feature Extraction Procedure

4.2 Defect Shape Restoration Capability Analysis

For circular corrosion defects serving as the reference standard, the experimentally measured circularity values range from 0.80 to 0.94. The minimum circularity value of 0.80 corresponds to a circular corrosion defect with a diameter of 5 mm. This low value is attributed to the susceptibility of boundary features in small-sized defects to interference during detection. Nevertheless, through the enhancement of raw data via signal sharpening and the PCHIP interpolation algorithm, combined with spatially constrained segmentation using k-means clustering, this approach accurately restores the shape of defects. Experimental results demonstrate that the method exhibits good robustness in preserving the original shape characteristics of the defects, validating its effectiveness in detecting minute defects.

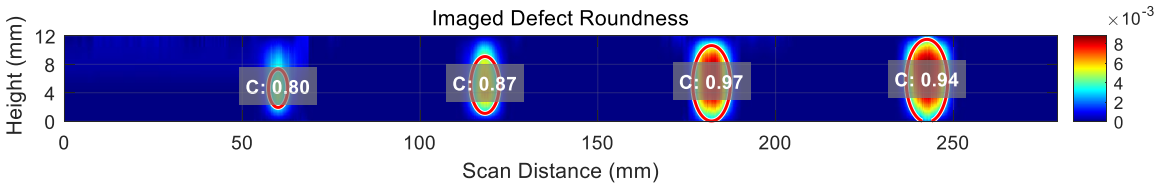


Fig. 12. Roundness Measurement of Defects

4.3 Impact of Sharpening on Defect Quantification Accuracy

The defect feature extraction results from the unsharpened raw signal are shown in Figure 13, while the corresponding quantitative analysis results (defect area recognition accuracy and coordinate positioning error rate) are presented in Figure 14. Experiments demonstrate that at the same burial depth, defect area is positively correlated with the peak amplitude of the detection signal. Consequently, for the defects studied in this paper (diameters of 5mm, 8mm, and 10mm), their signal peak amplitudes exhibit a clear increasing trend. However, due to the saturation of the eddy current probe's detection range, the peak signal amplitudes for the 10mm and 12mm diameter defects show no significant change. Within the effective detection capability of the probe, larger defect areas exert a greater influence on the detection outcome.

To enhance quantification accuracy, the sharpening exponent γ was adaptively adjusted based on the signal peak amplitude, and sharpening was applied to signals from corrosion defects of different sizes. This approach greatly enhanced defect quantification accuracy: the original method (without sharpening) achieved an average area recognition accuracy of less than 50% across the four defects. After optimization with adaptive power-law sharpening, the area recognition accuracy for the smallest defect (5mm diameter) increased to 83.7%, while the average accuracy for the other defect sizes (8–12mm diameter) exceeded 90%. Regarding coordinate positioning, the fusion method based on PCHIP interpolation and k-means clustering achieved fractional millimeter accuracy. The maximum centroid coordinate error was 1.5%, dropping to a minimum of 0.17% (for the 12mm diameter defect), with the average error stabilized at the 1% level.

This technical system, through the synergistic effects of sharpening for enhanced edge features, interpolation for optimized data distribution, and clustering for precise segmentation, successfully achieved high-precision quantitative analysis of both corrosion defect area and position coordinates. Even under the most unfavorable conditions, the area measurement error was controlled within 16.3%, and the coordinate positioning error remained below 1.5%. This provides an effective solution for the

precise quantitative assessment of small industrial corrosion defects.

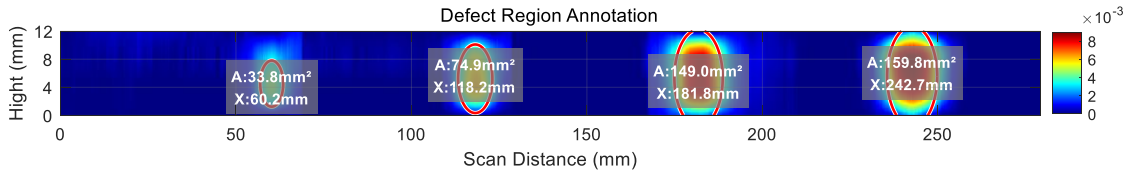
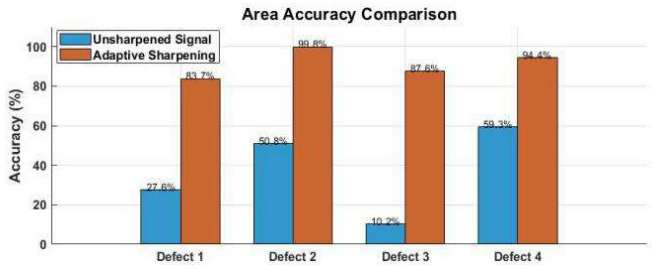
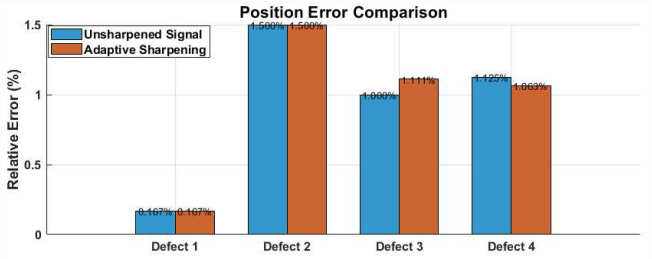


Fig. 13. Non-sharpened Defect Extraction



(a) Defect Area Accuracy



(b) Defect Coordinate Error Rate

Fig. 14. Area Accuracy vs. Coordinate Error Rates

5 Conclusion and future work

In summary, the proposed method resolves the key constraints of spatial broadening and low sampling resolution in PEC testing for multi-layer riveted structures. Through adaptive sharpening, high-density reconstruction, and unsupervised clustering, it offers a generalizable high-precision quantification framework, as validated by experiments.The main results and contributions are as follows.

1) Boundary localization enhancement. The proposed adaptive power-law sharpening algorithm dynamically modulates the exponent γ in accordance with normalized peak heights, thereby achieving intelligent compression of response envelope edges. Experimental results demonstrate a substantial improvement in defect boundary restoration accuracy, with particularly pronounced suppression of boundary blurring for micro-defects (e.g., 5 mm in diameter). This provides a critical foundation for subsequent quantitative analysis.

2) Resolution enhancement and automated segmentation. Leveraging the sharpened 4×n differential signal matrix, the method employs piecewise cubic Hermite interpolation (PCHIP) to

reconstruct a high-density data field, effectively overcoming the spatial resolution constraints of low-channel arrays. Concurrently, unsupervised K-means clustering enables automatic defect region identification and geometric parameter extraction. Validated on circular defects with diameters ranging from 5 mm to 12 mm, the proposed approach achieves an average post-optimization area recognition accuracy exceeding 90% (83.7% for the smallest 5 mm defects). Furthermore, the centroid localization error remains consistently below 1.5%, with an average error of approximately 1%.

3) Geometric reconstruction capability and future outlook. Under uniform burial depth conditions in multi-layer riveted structures, the method exhibits robust geometric reconstruction performance for micro-defects, achieving roundness ratios between 0.80 and 0.97, which indicates excellent immunity to boundary noise. It enables high-precision dual-parameter quantification of corrosion area and positional coordinates. For future work, the proposed framework will be extended to accommodate variable burial depths and irregular defect morphologies. Additionally, deep-learning-based adaptive parameter tuning will be explored to further enhance robustness and generalization in practical aircraft inspection scenarios.

Acknowledgment

This work was supported in part by the National Key R&D Program (No.2024YFB3214300), National Natural Science Foundation of China (No.12364056), Natural Science Foundation of Jiangxi Province (No.20253BAC280090, No.20252BAC240318)， Science and Technology Project of Jiangxi Administration for Market Regulation (No. GSJK202406).

Reference

[1] Yang Y T, Han Y, Yan H K, et al. Fatigue behavior of aircraft countersunk riveted joints under combined effects of hole diameter and squeeze force[J]. Engineering Failure Analysis, 2025, 179: 109810.

[2] JIA Jinghuan, SUN Zhihua, LUO Chen, et al. Research progress and development trend of corrosion detection technology for aviation equipment surfaces[J]. Corrosion & Protection (In Chinese), 2025, 46(07): 77-82.

[3] Song K, Ouyang Y, Fang Z, et al. Simulation and experiment of array remote-field eddy current sensor for hole edge defect of aircraft high lock bolt[J]. Acta Aeronautica et Astronautica Sinica, 2022, 43(5): 580-591.

[4] Bin Ali K, Abdalla A N, Rifai D, et al. Review on system development in eddy current testing and technique for defect classification and characterization[J]. IET Circuits, Devices & Systems, 2017, 11(4): 338-351.

[5] He K, Liang J, Yong J, et al. Quantitative detection of laser welding defective structure based on feature extraction of the pulsed eddy current signal[J]. Journal of Materials Engineering and Performance, 2023, 32: 6412-6422.

[6] Ge J, Xu F, Yusa N. Experimental investigation of low-frequency and pulsed eddy current testing in thickness measurement[J]. Nondestructive Testing and Evaluation, 2024, 40(11): 5271-5289.

[7] Fang J, Shen J, Xiong L, et al. Modelling and experimental study on pipeline defect characterisations using a pulsed eddy current measurement[J]. Nondestructive Testing and Evaluation, 2024, 40(9): 4024-4045.

[8] YANG Zhijun, ZHANG Zhiyong, BAI Tianxiang, et al. Coated pipeline wall thickness inversion technique based on pulsed eddy current[J]. Nondestructive Testing (In Chinese), 2025, 47(08): 52-56.

[9] Yan B, Li Y, Liu Z, et al. Pulse-modulated eddy current imaging for 3D profile reconstruction of subsurface corrosion in metallic structures of aviation[J]. IEEE Sensors Journal, 2021, 21(24): 28087-28096.

[10] SONG Kun, OUYANG Yong, FANG Zhou, et al. Influence of coil angle of PRFECT probe for aircraft riveted components[J]. Acta Aeronautica et Astronautica Sinica, 2021, 42(10): 406-415.

[11] Huang P, Bao Z, Guo J, et al. A thickness measurement method immune to lift-off fluctuation using sweep-frequency eddy current testing[J]. Journal of Nondestructive Evaluation, 2024, 44: 69.

[12] Wang R, Bao B, Wang W, et al. Research on remote-field eddy current focusing method for detecting hidden defects in aircraft riveted components[J]. Journal of Nondestructive Evaluation, 2023, 42: 95.

[13] Kopf L F, Tighe R C. Automated detection and quantification of the onset of undercoating corrosion using pulsed thermography[J]. Materials and Corrosion, 2023, 74(5): 777-792.

[14] Hernandez J, Fouliard Q, Vo K, et al. Detection of corrosion under insulation on aerospace structures via pulsed eddy current thermography[J]. Aerospace Science and Technology, 2022, 121: 107317.

[15] Stolze F H G, Worden K, Manson G, et al. Fatigue-crack detection in a multi-riveted strap-joint aluminium aircraft panel using amplitude characteristics of diffuse lamb wave field[J]. Materials, 2023, 16(4): 1619.

[16] Xu Z, Zhou Z, Chen H, et al. Effects of the wire mesh on pulsed eddy current detection of corrosion under insulation[J]. Nondestructive Testing and Evaluation, 2022, 38(2): 233-253.

[17] XU Hao, BAO Jun, HUANG Guoyong, et al. Simulation design of a novel eddy current probe for defect detection in aircraft multi-layer metal riveted structures[J]. Journal of Electronic Measurement and Instrumentation, 2024, 38(5): 178-187.

[18] WANG Anqi, ZHANG Jizhou, FAN Siwei, et al. Study on magnetic saturation pulsed eddy current method for liner collapse detection in bimetallic composite pipes[J/OL]. Engineering Mechanics, 1-13[2026-01-14].

[19] Xu Z, Zhu C, Jin J, et al. Reduction of pulsed eddy current probe footprint using sequentially excited multiple coils[J]. Journal of Nondestructive Evaluation, 2024, 43: 47.

[20] Yao W S, Ye Y F, Wang F H, et al. Pulsed eddy current testing method for corrosion thinning defects of ferromagnetic components based on parameter inversion algorithm[J]. Research in Nondestructive Evaluation, 2023, 34(5-6): 186-204.

[21] WANG Jin, LI Yong, SU Bingjie, et al. Pulsed eddy current visual inspection of subsurface corrosion defects in ferromagnetic metal plates based on dual-sensor differential mechanism[J]. China Mechanical Engineering, 2025, 36(03): 381-390.

[22] CUI Junjia, ZHANG Jun, SHAO Ruru, et al. Research on detection algorithm for offset defects in self-piercing riveting based on deep learning[J]. Aeronautical Manufacturing Technology, 2023, 66(6): 22-30.

[23] LI Guangyao, LIU Xiao, LAI Ming, et al. Research on intelligent detection algorithm for joint depth of magnetic pulse crimped tubes based on adaptive visual inspection[J]. Aeronautical Manufacturing Technology, 2022, 65(7): 54-63.

[24] Shao Q, Fan S, Liu F. Parameter optimisation of wavelet denoising for pulsed eddy current signals based on particle swarm optimisation algorithm[J]. Nondestructive Testing and Evaluation, 2023, 39(5): 1210-1224.

[25] Vu T P, Luong V S, Le M, et al. Hidden corrosion detection in aircraft structures with a lightweight magnetic convolutional neural network[J]. Nondestructive Testing and Evaluation, 2024, 40(5): 1797-1819.

[26] Sun C ,Yu Y ,Li H , et al.Quantitative Detection for Fatigue Natural Crack in Aero-Aluminum Alloy Based on Pulsed Eddy Current Technique[J].Applied Sciences,2024,14(10):4326-4326.

[27] Chen X ,Hou D ,Zhao L , et al.Study on defect classification in multi-layer structures based on Fisher linear discriminate analysis by using pulsed eddy current technique[J].NDT and EInternational,2014,67:46-54.

[28] Hosseini S ,Lakis AA .Application of time–frequency analysis for automatic hidden corrosion detection in a multilayer aluminum structure using pulsed eddy current[J].NDT and EInternational,2012,47:70-79.

[29] Yuan F, Yu Y, Wang W, et al. Pulsed eddy current array design and electromagnetic imaging for defects detection in metallic materials[J]. Nondestructive Testing and Evaluation, 2022, 37(1): 81-99.

[30] Su B, Li Y, Liu Z, et al. Near- and remote-field pulsed eddy current integrated testing for enhancement in imaging of buried flaws in layered conductive structures[J]. Nondestructive Testing and Evaluation, 2024, 40(8): 3517-3530.

[31] Sun G ,Hu M .Signal Processing and Defect Characterization of Pulsed Eddy Current Testing Based on Cross-Correlation[J].Procedia Computer Science,2022,208300-309.